

# Journal of Materials Chemistry A

Accepted Manuscript



This is an *Accepted Manuscript*, which has been through the Royal Society of Chemistry peer review process and has been accepted for publication.

*Accepted Manuscripts* are published online shortly after acceptance, before technical editing, formatting and proof reading. Using this free service, authors can make their results available to the community, in citable form, before we publish the edited article. We will replace this *Accepted Manuscript* with the edited and formatted *Advance Article* as soon as it is available.

You can find more information about *Accepted Manuscripts* in the [Information for Authors](#).

Please note that technical editing may introduce minor changes to the text and/or graphics, which may alter content. The journal's standard [Terms & Conditions](#) and the [Ethical guidelines](#) still apply. In no event shall the Royal Society of Chemistry be held responsible for any errors or omissions in this *Accepted Manuscript* or any consequences arising from the use of any information it contains.

# Ageing mechanisms of highly active and stable nickel-coated silicon photoanodes for water splitting†

Tingting Han,<sup>a,‡</sup> Yuanyuan Shi,<sup>a,‡</sup> Xiaoxue Song,<sup>a</sup> Antonio Mio,<sup>b</sup> Luca Valenti,<sup>b</sup> Fei Hui,<sup>a</sup> Stefania Privitera,<sup>b</sup> Salvatore Lombardo<sup>b</sup> and Mario Lanza<sup>a\*</sup>

<sup>a</sup>Institute of Functional Nano & Soft Materials, Soochow University, Collaborative Innovation Center of Suzhou Nanoscience and Technology, Suzhou, 215123, China

<sup>b</sup>Institute for Microelectronics and Microsystems, National Research Council (IMM-CNR), 533 Stradale Primosole 95121 Catania, Italy

\* Corresponding author e-mail: mlanza@suda.edu.cn

† Electronic supplementary information (ESI) available.

‡ These authors contributed equally to this work

KEYWORDS: Water splitting; Photoanode; Lifetime; Ageing mechanism; Nanofilament

## Abstract

The photoelectrochemical (PEC) water splitting cell, a device that uses sunlight to produce hydrogen, has raised massive interest due to its simple structure, low fabrication cost and good performance. In these cells, a semiconductor photoelectrode is immersed in a liquid and, when illuminated, hydrogen and/or oxygen can be generated on its surface by electrolysis. Metal catalysts are often used to enhance the activity of the semiconductor, but the lifetime is still the main bottleneck of this technology. In this manuscript we report the ageing mechanisms of silicon photoanodes coated with nickel films of different thicknesses (under light-driven oxygen evolution reaction, OER). The 2 nm, 5 nm and 10 nm nickel-coated n-Si photoanodes show lifetimes of ~18 h, ~150 h and >260 h, respectively. While the 2 nm sample degrades due to the formation of a highly resistive NiO<sub>x</sub> with abundant potassium contamination (from the electrolyte), the performance of the thicker samples decreased due to

the formation of holes. The 5 nm and 10 nm thick nickel films turned into an homogeneous potassium-free NiO<sub>x</sub> film suitable for water-splitting, which remarkably enhanced the performance of the cells. The density/size of holes in the surface decreased/increased with the metal thickness. The potassium contamination in the 2 nm Ni sample takes place in the form of nanofilaments, and we demonstrate that the widely used X-ray photoelectron spectroscopy tests are blind to these features, which may have been ignored in all previous reports. These results could be useful to understand the degradation and enhance the yield of water-splitting solar cells.

## 1. Introduction

The use of solar energy to produce storable and transportable clean fuels has attracted worldwide attention as renewable energy source,<sup>1,2</sup> as it solves the problems of sunlight intermittence and location dependency, while avoiding the use of contaminant and every time more scarce fossil fuels. A raising methodology allowing this conversion is the use of electricity generated in a photovoltaic system to break down water (H<sub>2</sub>O) into hydrogen and oxygen by electrolysis.<sup>3,4</sup> Due to its low cost and good ability to absorb light, silicon is one of the most preferred semiconductor photoelectrodes but, unfortunately, using semiconductor materials the amounts of hydrogen and oxygen produced are very modest, and the chemical reactions decay after some minutes due to surface corrosion. To overcome these problems, the most advanced water splitting cells use a catalyst and protective coating deposited directly on the semiconductor surface. Several metal-based catalysts including Ru,<sup>5</sup> Ni,<sup>6</sup> NiO<sub>x</sub>,<sup>7,8</sup> Ir,<sup>9</sup> Cu,<sup>10</sup> CuO<sub>x</sub>,<sup>11</sup> MnO<sub>x</sub><sup>12</sup> and Co<sup>13</sup> have been demonstrated to enhance the activity of semiconductor photoelectrodes for water splitting, achieving current densities up to tens of mA/cm<sup>2</sup>.<sup>7</sup> While cell activity amply exceeds the requirements of this technology, stability is still a major concern. Among all catalysts used, there is consensus that nickel based oxides and compounds are the best cost-effective and durable solution.<sup>6-8,14-17</sup> In our previous work, we observed that silicon photoanodes coated with ultrathin (2 nm) layers of nickel can

generate current densities of  $10 \text{ mA/cm}^2$  during more than 80 hours.<sup>6</sup> Recently, Mei et al.<sup>17</sup> achieved stable water splitting during 300 h using  $p^+n$  silicon photoanodes coated with 50 nm thick Fe-treated NiO films, and Sun et al.<sup>7</sup> reported lifetimes above 1200 h using even thicker 35~160 nm  $\text{NiO}_x$  films on  $np^+$  silicon. It is worth noting that the use of thick coatings reduces the light transmittance to the silicon, leading to larger onset potentials and smaller saturation currents.<sup>6</sup> Moreover, the fabrication of buried  $np^+$ -Si junctions involves additional processing steps during the manufacturing process.

Despite the long lifetimes reported, the ageing mechanisms that produce activity decay and device failure in water splitting solar cells are still not understood, and one of the main reasons is the important lack of in-depth reliability studies at the nano and atomic scales. The widely used scanning electron microscopy (SEM) is unable to provide clear-cut information about the samples, and it has been mainly used to display the thickness of the coatings<sup>6,7,17</sup> and to have a loose idea about surface roughness<sup>16</sup>. Surface roughness has been quantitatively analyzed by Atomic Force Microscope (AFM)<sup>7,14,15</sup>, but no work provides a thorough characterization depending on the testing time, precluding the detection of degradation trends and ageing mechanisms. X-ray photoelectron spectroscopy (XPS)<sup>18-20</sup>, energy-dispersive X-ray spectroscopy (EDS)<sup>16,17</sup> and Auger electron spectroscopy (AES)<sup>6</sup> have been widely used for chemical characterization, but the lateral resolution of these techniques is  $\sim 10 \mu\text{m}$ ,  $\sim 1 \mu\text{m}$  and  $\sim 20 \text{ nm}$  (respectively), and they can mask local phenomena and defects produced during PEC. Few groups reported the use of cross sectional Transmission Electron Microscope (X-TEM) to obtain information at the atomic level<sup>19,14,16,18,21</sup>, but only images of fresh samples are provided (to prove the thickness of the layers).

In this work we fabricate nickel-coated silicon photoanodes with long lifetimes above 260 hours, and we exhaustively analyze their ageing mechanisms at nano and atomic scales. Characterization tools traditionally used in the field of water splitting solar cells, such as SEM, XPS and AFM are combined with X-TEM, and we introduce for the first time the use of

Electron Energy Loss Spectroscopy (EELS) in the study of water splitting solar cells. Our results demonstrate that the ageing of the photoanodes is strongly linked to the thickness of the catalyst coating, and we report remarkable differences on surface roughness, stack homogeneity, conduction mechanisms and formation of defective holes.

## 2. Experimental Section

### 2.1. Fabrication of electrodes

As-received phosphorous-doped (100) n-type silicon wafers (from Prolog Semicor) with a resistivity of 0.3-0.5 Ohm·cm were cleaned using a three-steps process. First, the wafers were immersed in acetone for 10 minutes, then in ethyl alcohol for 10 minutes more, and finally in deionized water for another 10 minutes. For all cleaning steps, the ultrasonic bath was used. After that, the samples were dried with an N<sub>2</sub> gun. As reference, one n-Si sample was immersed in water-diluted hydrofluoric acid (HF:H<sub>2</sub>O volume ratio 1:5) for 10 seconds to remove the native oxide. Once the n-Si wafers were cleaned a thin layer of nickel (with a thicknesses of 2 nm, 5 nm or 10 nm) was evaporated on their top surface. On the back side of the wafer, 20 nm titanium was evaporated to form an Ohmic contact. The electron beam evaporator used was the PVD75 from Kurt J. Lesker at a deposition rates of ~0.15 Å/s and ~0.45 Å/s for the Ni and Ti layers, respectively. Copper tape was used to contact the Ti on the backside for electrochemical experiments.

### 2.2. Electrochemical characterization

The electrodes were tested in a square container with two circular apertures located at opposite faces, and with sizes of 0.5 cm<sup>2</sup> and 2 cm<sup>2</sup>. The small aperture was sealed by the electrode using a rubber ring and a back tap fixed by four screws. Similarly, the bigger aperture was sealed using a glass, through with a light flux was driven to the surface of the

electrode. The light flux was generated using a 150 W Xenon lamp from Newport Corporation, and the electrodes were irradiated using a light power density of  $\sim 50 \text{ mW/cm}^2$ , which was corroborated with an optical power meter from Newport Corporation (model 1918-R). A saturated calomel electrode (SCE, saturated KCl) was used as reference electrode, and a stainless steel electrode as counter electrode. Electrochemical experiments were performed in a three-electrode system controlled by a CHI 660E potentiostat. Before the experiments, the container was filled with an electrolyte consisting of 1 M potassium hydroxide (KOH, pH=14), prepared by dissolving 5.6 g KOH (from Sinopharm Chemical Reagent) in 100 mL deionized water. Before every measurement, bubbles were removed from the aperture using a plastic pipette. When testing the long-time I-t curves, the production of bubbles decreased the amount of electrolyte in the container, and more KOH was poured. Before and after the electrochemical tests, the electrical resistance of the system was registered. During the experiments, cyclic voltammetry (CV), linear sweep voltammetry (LSV) and amperometric I-t curves were measured. All CVs and LSVs were collected at 100 mV/s, and 10 mV/s, respectively.

### 2.3. Materials Characterization

After electrochemical characterization, the photoanodes were rinsed with water for 10 seconds, washed again in deionized water for 3 minutes and dried with the  $\text{N}_2$  gun. The morphological changes induced by the electrochemical tests were analyzed with two different the Scanning Electron Microscopes (SEM), the FEI Quanta 200FEG and the Zeiss SUPRA55, and also by means of Atomic Force Microscopy (AFM), using the MultiMode V from Veeco working in tapping mode and using NanoWorld Pointprobe tips (model NCH, item no. 78131F6L965). The chemical composition of the samples was analyzed with the X-ray Photoelectron Spectroscopy (XPS), model Shimadzu KRATOS AXIS Ultra DLD Scanning XPS Microprobe. Additionally, atomic scale morphologic and chemical information was gained combining cross-sectional Transmission Electron Microscopy (X-TEM) coupled with

the Electron Energy Loss Spectroscopy (EELS) acquired in scanning mode (STEM), using a JEOL JEM 2010F electron microscope with a 200 kV accelerating voltage. Between photoelectrochemical experiments and X-TEM analyses, the photoanodes were protected with 50 nm Au to avoid the effect of the environment. The Leica Microsystems (DM4000M) Fluorescence optical microscope was used to analyze the surface of the samples. The conductivity of fresh and tested photoanodes was analyzed at both the nanoscale and the device level. The electrical conductivity of the photoanodes has been measured using the Bruker Multimode VIII conductive AFM (CAFM), using Pt-varnished silicon tips from Nano World (model PPP-CONTPt, item no. 80064F11L1115). In order to characterize the photocurrents through the photoanodes, the current maps were collected under illumination (provided by the built-in laser of the CAFM) and without applying any external bias. For device level characterization, metallic electrodes made of 50 nm Au were evaporated directly on the surface of the Ni photoanodes using a laser-patterned shadow mask from Tecan (UK). The devices were characterized by collecting current-voltage (I-V) curves using a probe station (Cascade, model: M150) and a semiconductor parameter analyzer (Keithley, model: 4200-SCS). It is worth noting that the morphological characterization of the samples by AFM, SEM, TEM and EELS was performed ex-situ. Despite the surface of the samples in operation (in contact with the electrolyte) and during ex-situ characterization (in air or vacuum) may be different, the permanent damage induced by the PEC tests can be effectively demonstrated, as many other authors did.<sup>6, 9, 12</sup>

### 3. Results and discussion

N-type silicon wafers (with their native oxide) were coated, by electron beam evaporation, with nickel layers of different thicknesses (2 nm, 5 nm and 10 nm). The resulting photoanodes were tested under potassium hydroxide (KOH, pH = 14) in a three-electrode system, using a saturated calomel electrode (SCE) and a stainless steel counter electrode. Sequences of cyclic voltammograms (CV) and amperometric current-time (I-t) curves have been measured under

an illumination of  $50 \text{ mW/cm}^2$  and in the dark. Fig. 1a shows the schematic of the setup used to characterize the samples, and Fig. 1b is the X-TEM image of a 5 nm nickel-coated silicon photoanode. More details about fabrication and characterization processes can be found in the methods section and supplementary information.

Fig. 1c shows the typical CVs recorded for the three types of Ni/SiO<sub>x</sub>/n-Si photoanodes. The 2 nm Ni sample shows the lowest onset potential ( $\sim 80 \text{ mV vs. SCE}$ ) and the largest saturation currents ( $\sim 10 \text{ mA/cm}^2$  under  $50 \text{ mW/cm}^2$ ), due to the higher light transmittance into the silicon.<sup>6,21</sup> As reference, the 2 nm Ni layer was also deposited on a native-oxide-free n-Si photoanode (after etching the native SiO<sub>2</sub> by HF solution). As we can observe in Fig. S2†, the current of this photoanode decreases after each CV scan, which indicates that the native SiO<sub>2</sub> is necessary for ensuring good cell stability. It has been suggested that the SiO<sub>2</sub> layer may work as adhesive to retain the Ni.<sup>6</sup> The short time I-t curves (Fig. 1d) reveal stable currents during the first two hours for all samples, showing the characteristic saw tooth shape related to oxygen bubble formation during OER (see Fig. S3†).

The lifetime and ageing mechanisms of the photoanodes are analyzed by means of long time PEC tests. Fig. 2a shows representative I-t curves for 5 nm and 10 nm nickel-coated silicon electrodes tested during different times. In total four 5 nm and three 10 nm nickel photoanodes (fabricated in three different batches) were measured. As it can be observed, the 5 nm sample shows stable currents during 6.5 days, and after that the current signal linearly decreases. Fig. 2b and 2c correspond to the SEM and AFM images collected on 5 nm Ni samples after different testing times. The initial root mean square (RMS) roughness of the fresh 5 nm nickel layer is 0.147 nm (which is very similar to that of bare silicon<sup>22</sup>) and it increases with the testing time, reaching 2.66 nm after 3.5 days. Interestingly, this morphological change didn't degrade the performance of the sample, indicating the formation of a rough layer able to split water. For longer times, both the SEM and AFM images reveal the progressive formation of defective holes, and after 6.5 days, the density of holes is

prohibitive and the performance of the cell starts to decay linearly. After 10 days, the SEM images show the typical picture of a silicon substrate etched by KOH,<sup>6</sup> (see also Fig. S4†) indicating that the nickel coating was completely etched. This is further supported by a dramatic increase of the sample roughness in the AFM maps. The chemical composition of this sample is analyzed by means of XPS (Fig. S5†). The spectra collected after different testing times reveal a change on the nickel ( $\text{Ni}^0$  to  $\text{Ni}^{3+}$ ) and oxygen peaks, indicating the formation of an effective  $\text{NiO}_x$  layer after 24 h PEC test. The XPS data also reveal the presence of potassium from the electrolyte after the test. The absence of a strong silicon signal indicates the presence of the coating after 24 h PEC test (in agreement with the SEM pictures, which show corrosion only after 6.5 days).

These observations are corroborated by means of X-TEM and EELS, which provide morphological and chemical information with sub-nanometer lateral resolution. Fig. 3a and 3b show the X-TEM pictures for the 5 nm sample before and after 24 h PEC test, respectively. The nickel layer in the fresh sample shows polycrystalline structure, and its thickness is very close to the theoretical one indicated to the evaporator. After the test, the thickness of the coating increases up to 6 nm, although nanometer scale statistical variability related to roughness deviations should be not discarded (see Fig. S6†). The chemical maps obtained with EELS (Fig. 3c) indicate the Ni coating transformed into  $\text{NiO}_x$ , which furthermore is very homogeneous. The surface of the sample tested for 24 h (Fig. 3b) also reveals the formation of a very thin bright layer on top of the  $\text{NiO}_x$ , which is probably related to the potassium from the electrolyte, as suggested by the XPS data (Fig. S5c†). In any case, the bulk of the  $\text{NiO}_x$  coating seems to be free of impurities. The volume expansion in the  $\text{NiO}_x$  film was expected, since it is known that oxygen evolution is preceded by three-dimensional oxide film formation,<sup>23</sup> on which discharge of OH and/or O takes place. It should be noted that the thickness of the interfacial native  $\text{SiO}_x$  film experienced a small thickness increase of typically  $\sim 0.4$  nm.

The 10 nm nickel-coated sample shows stable photocurrents during the whole 11 days tests (Fig. 2a). As for the 5 nm nickel electrode, a clear roughness increase can be easily observed after some hours test (Fig. S7a†), again corroborating the formation of a rough layer that is able to split water. In this case, the sample shows a much longer lifetime (above 11 days) when exposed to continuous OER, and most of the sample surface shows holes-free morphology (Fig. S7b†). The thicker nature of the layer probably reduced the initial density of pinholes,<sup>24</sup> leading to a less ion-permeable layer that is less susceptible to corrosion.

Similar experiments were performed for the 2 nm nickel-coated samples. Fig. 4a shows the I-t curves collected after 8 h, 11 h, 15 h, 28 h and 57 h OER tests for five 2 nm nickel photoanodes fabricated in three different batches, showing excellent repeatability and small variability. Interestingly, the degradation process of all 2 nm nickel photoanodes show important differences compared to the 5-10 nm ones, and three characteristic degradation steps can be distinguished: *I*) slow current decay during the first 7 hours; *II*) severe current degradation between the hours 7<sup>th</sup> and 11<sup>th</sup>; and *III*) slow decay with a slope similar to that observed in the first step. Again, both SEM and AFM images (Fig. 4b and 4c respectively) reveal an increase of the surface roughness with the testing time: the initial roughness (0.11 nm) progressively increased up to 2.86 nm after 57 hours. During this degradation process, there are two factors that should be highlighted: i) the final roughness of the sample (2.86 nm) is much smaller than the one measured for the 5 nm Ni sample (102 nm), and also smaller than that of a piece of silicon corroded by KOH (24.07 nm in Fig. S4†); and ii) the SEM images don't reveal the formation of large defective holes in the catalyst (see Fig. 4b).<sup>6,8</sup> The absence of holes during the first 57 hours test is further corroborated by exposing the samples to even longer water splitting tests, which revealed that defective holes started to appear on the electrode only after 3 days (see inset in Fig. 4b and Fig. S8a†). Sun et al.<sup>7</sup> associated the formation of holes to silicon corrosion through small pores and/or grain boundaries in the NiO<sub>x</sub> film. Our sequences of SEM images provide new insights on the formation of defective holes: the average diameter of the holes increases with the thickness of the nickel coating (Fig.

S8†), and the sizes for each nickel thickness show relatively low variability (i.e. the largest holes for the 2 nm sample are always smaller than the smallest holes in the 5 nm one).

The absence of holes in the 2 nm samples before 3 days indicates that the degradation of the cells is not related to the apparition of defective holes during OER, but it is linked to the formation of a rough layer unable to split water. It is worth noting that the 5-10 nm samples maintained the initial saw tooth shape during the whole degradation process (see Fig. S9b†), while in the 2 nm samples the initial saw tooth shape for bubble formation changed into sharp peaks (see Fig. S9a†), indicating a change in the conduction mechanisms through the photoanode. This behavior was in-depth analyzed at the nanoscale and device level using the CAFM and the probestation (respectively). Figs. 5a and 5d show the CAFM current maps of the fresh and tested 2 nm Ni/SiO<sub>x</sub>/n-Si photoanode (under illumination and without bias). The abundant photocurrents observed in fresh samples completely vanished in the sample exposed to OER during 16 hours. For the device level characterization, squared Au electrodes of different sizes were patterned on the fresh and tested samples using a shadow mask and an evaporator (Fig. 5b and 5e). The measured IV curves collected on the fresh samples (Fig. 5c) show typical photocurrent at 0V, as well as an open-circuit voltage of ~ 60 mV. On the contrary, the sample exposed to 16 hours OER shows almost negligible photocurrent and open-circuit potential, as well as much smaller currents at high biases (Fig. 5f), indicating that the conductivity of the photoanode has been dramatically reduced.

The XPS analysis (Fig. S10†) of the 2 nm Ni samples didn't reveal any significant change compared to the 5 nm ones: the nickel, oxygen and potassium profiles are very similar, and the only remarkable change is the larger silicon signal, due to the smaller thickness of the nickel coating. Interestingly, there is a correlation between the potassium signal and the degradation of the sample. Further observations were made when the sample was analyzed with X-TEM and EELS. Again, the fresh sample showed correct thickness, chemical composition and polycrystalline structure (Fig. 6a and 6c). After 1 h, the X-TEM images

clearly display the roughness increase. Fig. 6b intentionally shows a part of the sample that is specially corroded, and the local changes on the morphology of the material are clearly identified (see inset). Interestingly, in this case the interfacial native  $\text{SiO}_x$  film experienced a much larger thickness increase, leading to an effective film always thicker than 3 nm. Such a thick insulating layer should be the main factor limiting the conduction from the electrolyte to the silicon substrate, as observed in Figs. 5d and 5f, and producing the activity decay (Fig. 4a). After 24 hours test (Fig. 6c), the thickness of the Ni layer increased up to 4.6 nm, the film became darker and, interestingly, some light nanofilaments connecting both sides of the coating can be distinguished. The EELS chemical profiles (sections A-A' and B-B', displayed in Fig. 6e and 6f, respectively) reveal the formation of a  $\text{NiO}_x$  layer rich in potassium on its surface (Fig. 6e), in clear agreement to the XPS data. The large lateral resolution of this technique allowed to assess the chemical composition of the light nanofilaments, revealing that they are rich in potassium, which can penetrate in the nickel layer and reach the underlying  $\text{SiO}_x$  layer (Fig. 6f). Fig. 6f shows that the Ni concentration is reduced when the potassium signal increases, indicating that the potassium is present only where pinholes are formed. We speculate that pinholes nucleated at defects in the Ni surface, which becomes rough and rich of defects after a few hours of operation, and punch through the whole Ni layer and reach the Si/ $\text{SiO}_2$  surface. Then, the KOH solution starts to etch the Si layer below, as consequence of the well known large etching rate of KOH on (100) Si due to the  $\text{OH}^-$  ions. In the case of 5 nm and 10 nm, the increased Ni thickness is beneficial for extending the operation lifetime, since the pinholes have to pass through a thicker film. The unprecedented observation of local potassium filaments in the 2 nm Ni coated sample demonstrates that XPS may mask essential information involved in the degradation process of the samples, and future investigations should include such kind of analyses.

#### 4. Conclusions

In summary, the degradation process of Ni/SiO<sub>x</sub>/n-Si photoanodes under light-driven OER has been analyzed using sub-nanometer characterization tools. The main conclusions of our work are: i) the activity/lifetime of the cells is lower/longer using thick Ni coatings; ii) 2 nm nickel coated samples fail within ~18 hours due to the formation of a thick interfacial SiO<sub>x</sub> film, which blocks hole/electron transfer to the electrolyte/substrate. Also, abundant potassium impurities penetration in the NiO<sub>x</sub> layer have been detected; iii) 5 nm and 10 nm nickel coated samples showed stable currents during more than ~150 and ~ 260 hours, respectively. In this case the Ni films also turned into NiO<sub>x</sub>, but the resulting layer was very homogeneous and free of impurities. The degradation of these samples was related to the formation of holes in the active NiO<sub>x</sub> layer, and the size/density of holes depends on its thickness; and iv) we demonstrate that essential information is masked in the XPS profiles, as the potassium contamination in the NiO<sub>x</sub> film can only be detected by combining TEM and EELS, indicating that previous reports in the field of water-splitting (which normally use traditional characterization tools with low spatial resolution) may be ignoring essential degradation phenomena. These findings may be of interest for the water-splitting community, as they reveal essential information that could be useful to enhance the lifetime of the cells.

### Acknowledgement

This work has been partially supported by the Young 973 National Program of the Chinese Ministry of Science and Technology (grant no. 2015CB932700), the Major State Basic Research Development Program of China (grant no. 2011CB013101), the National Natural Science Foundation of China (grants no. 11225208, 11521202, 11172001, 10872003, 10932001, 11072230 and 11375127), and the Natural Science Foundation of Jiangsu Province (grant BK20130280). The Project Funded by the Priority Academic Program Development of Jiangsu Higher Education Institutions (PAPD) is also acknowledged. Professor Mario Lanza acknowledges generous start-up funding from Soochow University

and from the "Young 1000 Talent Program" of China. M.J. Kenney from Stanford University is also acknowledged for results discussion.

## References

- 1 T.R. Cook, D.K. Dogutan, S.Y. Reece, Y. Surendranath, T.S. Teets, D.G. Nocera, *Chem. Rev.* 110 (2010) 6474-6502.
- 2 M.G. Walter, E.L. Warren, J.R. McKone, S.W. Boettcher, Q. Mi, E.A. Santori, N.S. Lewis, *Chem. Rev.* 110 (2010)6446-6473.
- 3 A.W. Bott, *Current Separations* 17 (1998) 87-91.
- 4 Z.B. Chen, H.N. Dinh, E. Miller, *SpringerBriefs in Energy*, first ed., Springer, New York, 2013.
- 5 L. Li, L.L. Duan, Y.H.Xu, M. Gorlov, A. Hagfeldt, L.C. Sun, *Chem. Commun.* 46 (2010) 7307-7309.
- 6 M.J. Kenney, M. Gong, Y.G. Li, J.Z. Wu, J. Feng, M. Lanza, H.J. Dai, *Science* 342 (2013) 836-840.
- 7 K. Sun, M.T. McDowell, A.C. Nielander, S. Hu, M.R. Shaner, F. Yang, B.S. Brunschwig, N.S. Lewis, *J. Phys. Chem. Lett.* 6 (2015) 592-598.
- 8 K. Sun, F.H. Saadi, M.F. Lichterman, W.G. Hale, H. Wang, X.H. Zhou, N.T. Plymale, S.T. Omelchenko, J. He, K.M. Papadantonakis, B.S. Brunschwig, N.S. Lewis, *Proc. Natl. Acad. Sci. USA* 112 (2015) 3612-3617.
- 9 Y.W. Chen, J.D. Prange, S. Dühnen, Y. Park, M. Gunji, C.E.D. Chidsey, P.C. McIntyre, *Nat. Mater.* 10 (2011) 539-544.
- 10 J. Du, Z. Chen, S. Ye, B.J. Wiley, T.J. Meyer, *Angew. Chem. Int. Ed.* 54 (2015) 2073-2078.
- 11 F. Yu, F. Li, B. Zhang, H. Li, L. Sun, *ACS Catal.* 5 (2015) 627-630.
- 12 N. C. Strandwitz, D.J. Comstock, R.L. Grimm, A.C. Nichols-Nielander, J. Elam, N.S.

- Lewis, J. Phys. Chem. C 117 (2013) 4931-4936.
- 13 V. Artero, M. Chavarot-Kerlidou, M. Fontecave, *Angew. Chem. Int. Ed.* 50 (2011) 7238-7266.
- 14 K. Sun, N. Park, Z.L. Sun, J.G. Zhou, J. Wang, X.L. Pang, S.H. Shen, S.Y. Noh, Y. Jing, S. Jin, P.K.L. Yua, D.L. Wang, *Energy Environ. Sci.* 5 (2012) 7872-7877.
- 15 K. Sun, S.H. Shen, J.S. Cheung, X.L. Pang, N. Park, J.G. Zhou, Y.F. Hu, Z.L. Sun, S.Y. Noh, C.T. Riley, P.K.L. Yu, S. Jine and D.L. Wang, *Phys. Chem. Chem. Phys.* 16(2014) 4612-4625.
- 16 S. Hu, M.R. Shaner, J.A. Beardslee, M. Lichterman, B.S. Brunshwig, N.S. Lewis, *Science* 344 (2014) 1005-1009.
- 17 B. Mei, A.A. Permyakova, R. Frydendal, D. Bae, T. Pedersen, P. Malacrida, O. Hansen, I.E.L. Stephens, P.C.K. Vesborg, B. Seger, I. Chorkendorff, *J. Phys. Chem. Lett.* 5 (2014) 3456-3461.
- 18 K. Jun, Y.S. Lee, T. Buonassisi, J.M. Jacobson, *Angew. Chem. Int. Ed.* 51 (2012) 423427.
- 19 J.H. Yang, K. Walczak, E. Anzenberg, F.M. Toma, G.B. Yuan, J. Beeman, A. Schwartzberg, Y.J. Lin, M. Hettick, A. Javey, J.W. Ager, J. Yano, H. Frei, I.D. Sharp, *J. Am. Chem. Soc.* 136 (2014) 6191-6194.
- 20 B. Mei, B. Seger, T. Pedersen, M. Malizia, O. Hansen, I. Chorkendorff, P.C.K. Vesborg, J. Phys. Chem. Lett. 5 (2014) 1948-1952.
- 21 A.G. Scheuermann, J.D. Prange, M. Gunji, C.E.D. Chidseyb, P.C. McIntyre, *Energy Environ. Sci.* 6 (2013) 2487-2496.
- 22 C. Gui, M. Elwenspoek, N. Tas, J.G.E. Gardeniers, *J. Appl. Phys.* 85 (1999) 7448-7454.
- 23 B.E. Conway, T.C. Liu, *J. Chem. Soc., Faraday Trans.1* 83 (1987) 1063-1079.
- 24 M. Miyazaki, H. Hirayama, *Surf. Sci.* 602 (2008) 276-282.

**Figure captions**

**Fig. 1.** Fabrication and characterization of Ni/SiO<sub>x</sub>/n-Si photoanodes. (a) 3D schematic of the setup used to characterize the photoanodes. (b) Cross sectional TEM image of a fresh 5 nm Ni/SiO<sub>x</sub>/n-Si photoanode. (c) Typical cyclic voltammograms measured for the Ni/SiO<sub>x</sub>/n-Si photoanodes with Nickel thicknesses of 2 nm, 5 nm and 10 nm, tested in 1 M KOH under illumination of 50 mW/cm<sup>2</sup>. (d) Short time amperometric I-t curves measured at the constant potential of 1.8 V vs. SCE for the three Ni/SiO<sub>x</sub>/n-Si photoanodes with different Ni thicknesses.

**Fig. 2.** Degradation process of 5 nm and 10 nm Ni coated silicon photoanodes. (a) Representative amperometric I-t curves measured at the controlled potential of 1.8 V vs. SCE for the 5 nm and 10 nm Ni/SiO<sub>x</sub>/n-Si/Ti photoanodes in 1 M KOH under illumination of 50 mW/cm<sup>2</sup>. (b) and (c) show the SEM and AFM images collected after different testing times for the 5 nm Ni coated silicon photoanodes. The images of the fresh samples are also shown as reference. The 5 nm sample shows the formation of a rough layer that, unlike for the 2 nm Ni sample, is able to split water, and the sample only degrades when the density of holes is critical (after 6.5 days).

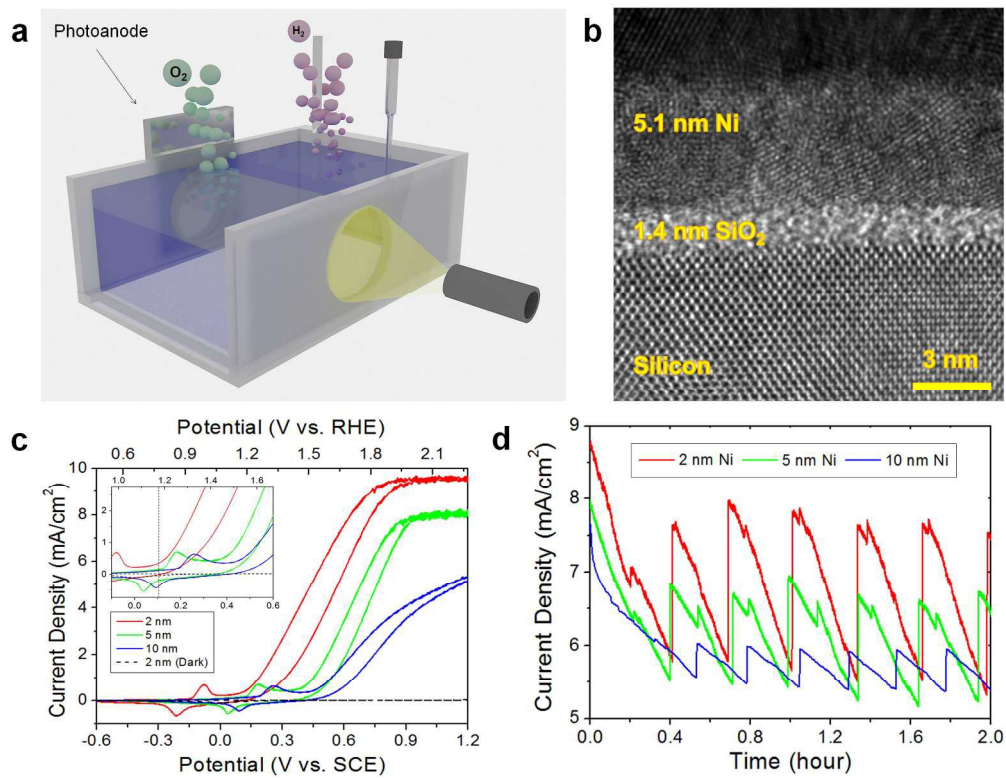
**Fig. 3.** Atomic scale information of fresh and tested 5 nm Ni coated silicon photoanodes. Cross sectional TEM images for the 5 nm Ni/SiO<sub>x</sub>/n-Si sample (a) before and (b) after 24 hours PEC tests. (c) Oxygen and nickel maps collected with EELS on the sample tested after 24h. The relative thickness increase is smaller and the formation of an effective NiO<sub>x</sub> layer is proved.

**Fig. 4.** Degradation process of 2 nm Ni coated silicon photoanodes. (a) Amperometric I-t curves measured at the constant potential of 1.8 V vs. SCE on five different 2 nm Ni/SiO<sub>x</sub>/n-Si/Ti photoanode during different times in 1 M KOH under an illumination of 50

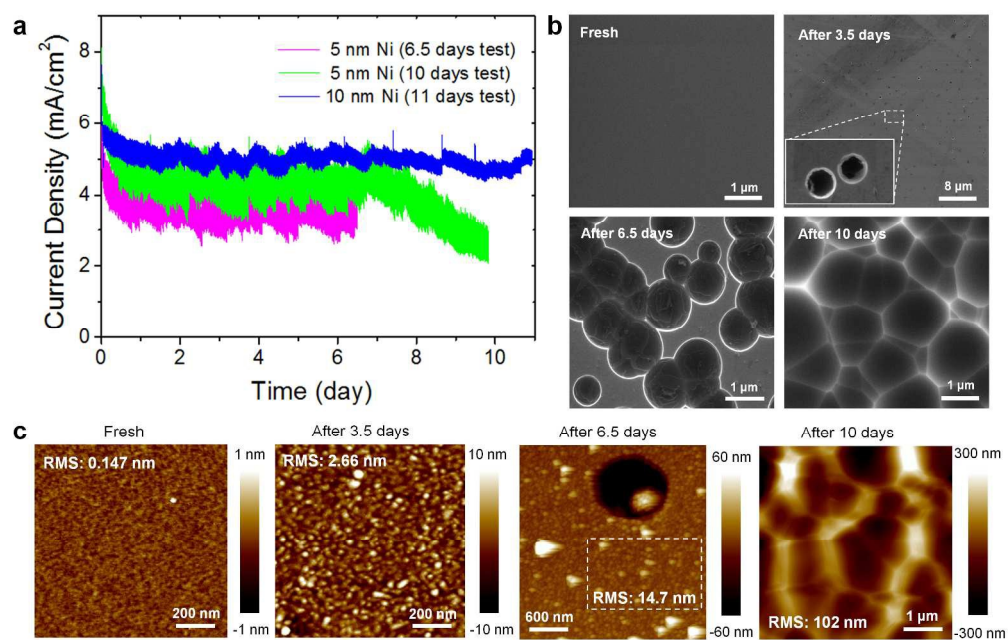
mW/cm<sup>2</sup>. The degradation of the sample takes place in three steps clearly distinguished (I, II and III). The inset shows the magnification of the first step, and excellent reproducibility can be observed. (b) and (c) show the SEM and AFM images collected on the Ni coated silicon photoanodes after different testing times. The images of the fresh samples are also shown as reference. The sample shows dramatic degradation after 57 hours test, which is accompanied by a roughness increase, but almost no holes were detected (they appeared only after three days test).

**Fig. 5.**Electrical characterization of the 2 nm Ni coated silicon photoanodes. CAFM current maps of the 2 nm Ni/SiO<sub>x</sub>/n-Si photoanode before (a) and after (d) continuous OER during 16 hours. The maps were obtained without bias and under illumination. (b) and (e) show the SEM images of the patterned squared electrodes on the fresh and tested samples (respectively). (c) and (f) show the I-V curves collected with the probestation for the fresh and tested samples (respectively). The black/red lines correspond to the I-V curves collected in the dark/illumination. The I-V curves shown in (c) and (f) were collected at the capacitors highlighted with green spots in (b) and (e).

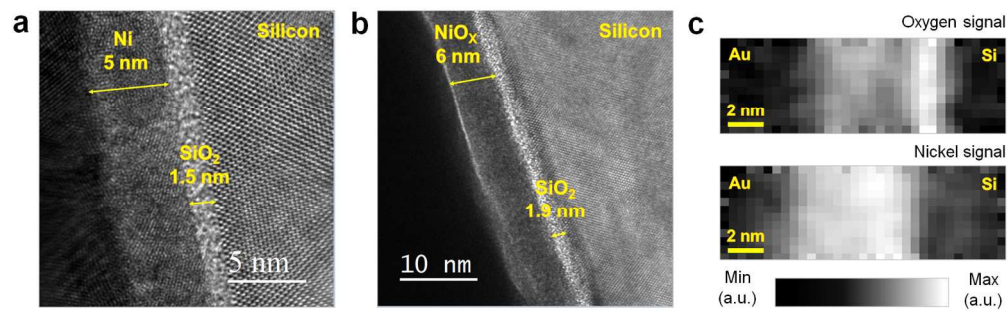
**Fig.6.**Atomic scale information of fresh and tested 2 nm Ni coated silicon photoanodes. Cross sectional TEM images for the 2 nm Ni/SiO<sub>x</sub>/n-Si sample (a) before the PEC tests, (b) after 1 hour test and (c) after 24 hours test. Panel (b) has been intentionally collected in a location that shows high surface roughness and film modification. (d) shows the EELS chemical composition of the fresh sample. (e) and (f) show the EELS chemical composition of the sample tested after 24 hours test, along the sections of a dark and a light region in (c).



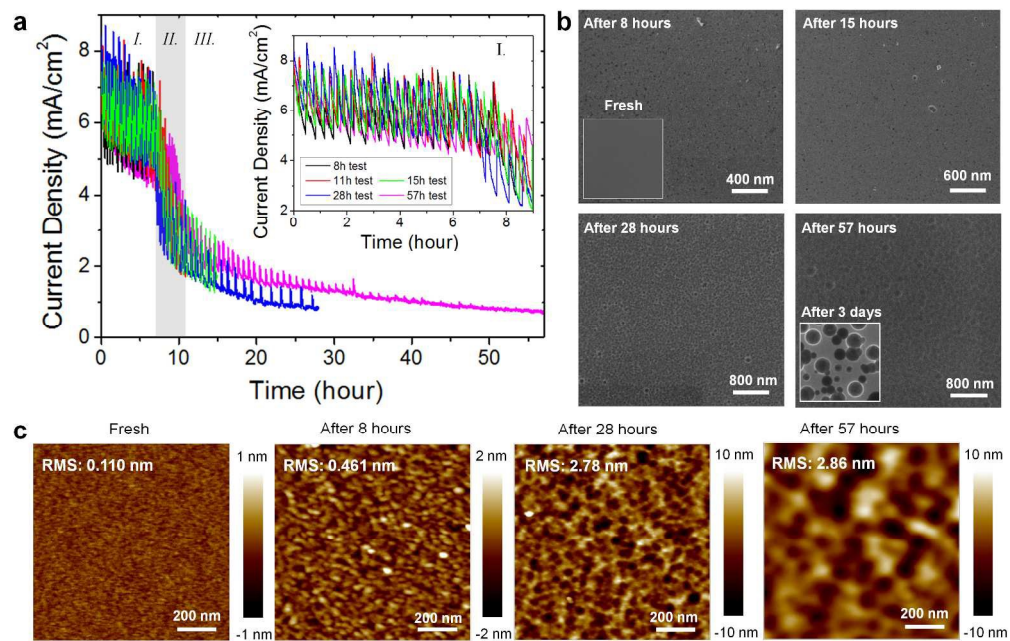
652x504mm (96 x 96 DPI)



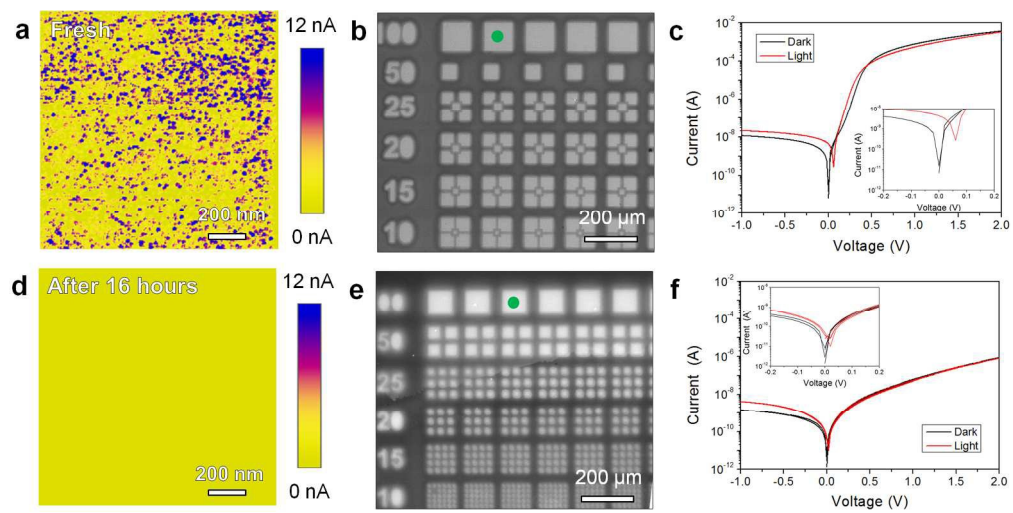
801x508mm (96 x 96 DPI)



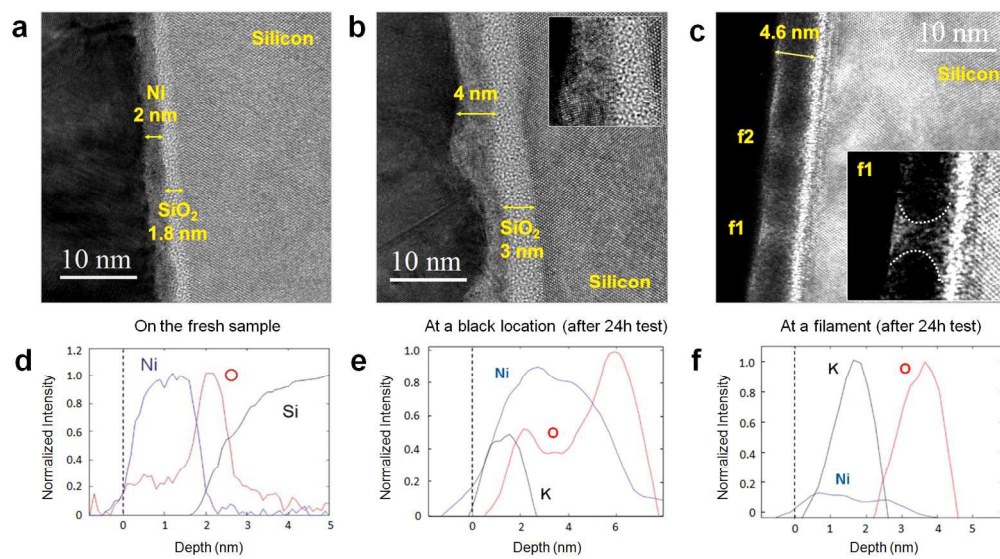
406x123mm (120 x 120 DPI)



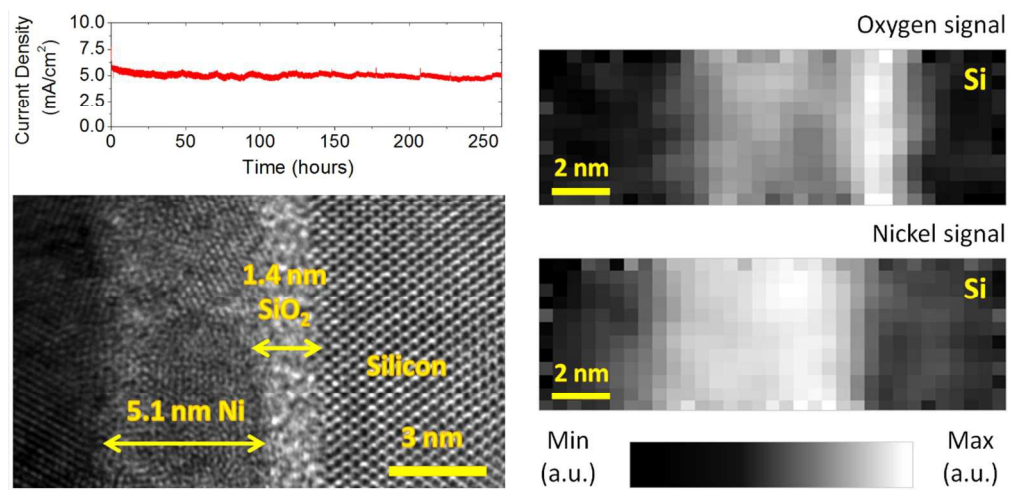
803x515mm (96 x 96 DPI)



569x284mm (96 x 96 DPI)



413x227mm (120 x 120 DPI)



339x162mm (96 x 96 DPI)